PCCP

PAPER

View Article Online
View Journal | View Issue

Cite this: *Phys. Chem. Chem. Phys.*, 2019, **21**, 2651

Distinctive phase separation dynamics of polymer blends: roles of Janus nanoparticles†

Qing Li, Liquan Wang, * Jiaping Lin * and Liangshun Zhang

Received 16th October 2018,
Accepted 2nd January 2019

DOI: 10.1039/c8cp06431h

rsc.li/pccp

Janus nanoparticles (JPs), which are anisotropic nanoparticles with at least two opposite surface regions, have been demonstrated as highly efficient compatibilizers for polymer blends. However, there are still a number of open questions concerning the mechanism behind the influence of JPs on the phase separation dynamics of polymer blends. Herein, we report a counter-intuitive feature of JPs concerning their roles during spinodal decomposition (SD); that is, they promote the decomposition of unlike polymers in the early stage of SD but retard it during the late stage. This is in remarkable contrast to traditional compatibilizers such as block copolymers and homogenous nanoparticles, which impede phase separation during both stages. We further demonstrate that the unique promoting effect of JPs at early times is due to the formation of microphase-separated homopolymer-rich regions in the vicinity of opposite JP surface regions. Our findings are expected to have important implications for the phase separation behavior of JP-compatibilized polymer blends, whose morphologies and performance could be controlled by tuning the interactions between the constituent polymers and JP-based compatibilizers.

1. Introduction

Janus nanoparticles (JPs) are anisotropic nanoparticles bearing at least two chemically different constituent parts.[1] Due to their unique physical and chemical properties, they have found applications in a number of fields, such as catalysts,[2,3] nanomotors,[4–6] drug delivery systems,[7,8] nanoimaging and nanosensors,[9–11] *etc.* Specifically, they have been demonstrated to be superior compatibilizers in comparison to traditional compatibilizers such as block copolymers and homogeneous particles,[12–21] because their unique combination of amphiphilicity and particulate nature (Pickering effect) favors strong and selective adsorption to interfaces.[22] When incorporated into heterogeneous blends, JPs can exclusively localize at the interfaces, thereby dramatically reducing the interfacial tension and preventing coalescence of the dispersed domains (droplets). Moreover, the impact of JPs on the phase separation dynamics of polymer blends has also attracted considerable attention. Huang *et al.* demonstrated that the segregation of Janus particles at the interfaces between polymer domains effectively reduces the number of unfavorable interactions, which leads to retarded domain growth during the late stage of spinodal decomposition (SD).[23,24] Their work provides valuable insights into the phase separation dynamics of JP-compatibilized blends, but research in this field is far from complete.

One of the challenges of both scientific and technological relevance is to comprehend the influence of JPs on the phase separation dynamics of polymer blends during the early stage of SD, which occurs when a mixture is quenched from the one-phase region in the phase diagram to the two-phase region.[25–28] During the early stage of SD, diffusional fluxes result in the development of a dominant composition fluctuation (SD wave) in the system, which later evolves into interface-separated domains that grow *via* the self-similarity mechanism during the late stage.[29,30] Therefore, investigating the role of Janus particles during the early stage may provide useful knowledge for controlling the morphology (and hence properties) of materials based on JP-compatibilized blends. However, experimental studies in this area are largely limited by difficulties with characterization and challenges in the large-scale preparation of JPs with well-defined structures.[1] Moreover, the nontrivial effect of long-range hydrodynamic interactions at early times makes it challenging to theoretically study early-stage phase separation.[31–33]

In the present work, the phase separation dynamics of JP-compatibilized blends during the full course of SD was studied *via* dissipative particle dynamics (DPD) simulations. This strategy is suitable for studying the phase behaviour of complex fluids because it offers large time and length scales, over which the effects of long-range hydrodynamic interactions can be correctly preserved.[34–40] We found that Janus particles uniquely exert opposite influences on the phase separation dynamics during the early and late stages, *i.e.*, they promote phase separation at

Shanghai Key Laboratory of Advanced Polymeric Materials, State Key Laboratory of Bioreactor Engineering, Key Laboratory for Ultrafine Materials of Ministry of Education, School of Materials Science and Engineering, East China University of Science and Technology, Shanghai 200237, China. E-mail: jlin@ecust.edu.cn, lq_wang@ecust.edu.cn

† Electronic supplementary information (ESI) available. See DOI: 10.1039/c8cp06431h

early times but impede it at late times. This result is in remarkable contrast to other compatibilizers such as block copolymers and homogenous particles, which usually impede phase separation during both stages. The present work not only deepens our understanding of the phase separation behaviour of JP-compatibilized blends but also offers a novel perspective for the investigation of chemically anisotropic nanoparticles.

2. Methods and models

2.1 Dissipative particle dynamics

Dissipative particle dynamics (DPD) is a particle-based technique for mesoscopic simulations.[34,41–44] A number of studies have demonstrated that it is particularly suitable for studying the phase separation behaviour of fluidic systems because the effect of long-range hydrodynamic interactions can be correctly preserved.[23,24,30,45,46] In this method, the movement of each bead is governed by the equations of motion $d\mathbf{r}_i/dt = \mathbf{v}_i$ and $m d\mathbf{v}_i/dt = \mathbf{f}_i$, where t is the time, m is the mass of each bead, $\mathbf{r}_i$ and $\mathbf{v}_i$ are the position and velocity of the ith bead, respectively, and $\mathbf{f}_i$ is the force applied to the bead. $\mathbf{f}_i$ consists of four parts, *i.e.*, a conservative force $\mathbf{F}_{ij}^{C}$, a dissipative force $\mathbf{F}_{ij}^{D}$, a random force $\mathbf{F}_{ij}^{R}$, and a spring bond force $\mathbf{F}_{ij}^{S}$. All forces are truncated at the cut-off radius, r_c. Specifically, the adjacent beads in the homopolymer chains and JP grafting blocks are connected *via* the spring bond force $\mathbf{F}_{ij}^{S} = C(1 - r_{ij}/r_{eq})\hat{\mathbf{r}}_{ij}$ where C is the spring constant, r_{eq} is the equilibrium distance, and $\hat{\mathbf{r}}$ is the unit vector pointing from the jth bead to the ith bead. The units of time, length, mass and energy are defined by τ, r_c, m and k_BT, respectively, where k_B is the Boltzmann constant, T is the temperature, and $\tau = (mr_c^2/k_BT)^{1/2}$. The magnitude of spring constant C was chosen to be 30, and the equilibrium distance r_{eq} was set at $0.86r_c$. The equations of motion were integrated *via* a modified velocity-Verlet algorithm with the time step $\Delta t = 0.02\tau$. (Detailed information on the DPD method is available in Section 1 of the ESI.†)

2.2 Models

The blending system studied here contains three components: homopolymer **A**, homopolymer **B**, and a core–shell Janus nanoparticle (JP) with a particulate **C** core grafted with equal numbers of **A** and **B** chains (see Fig. 1a–c). For conciseness, homopolymers **A** and **B** are denoted as P_A and P_B, respectively; the **A** and **B** grafting chains on the JPs are denoted as J_A and J_B, respectively; and the **C** core of the nanoparticle is denoted as J_C. In this work, identical volume fractions were maintained for P_A and P_B, while the volume fraction (c_{JP}) of the JPs was varied from 0 to 0.5. The interaction parameters a_{ij} (see eqn (S3), ESI†) between components **A**, **B** and **C** are given in Table 1. The parameters were defined to reproduce phase separation between unlike components.[43]

The models of P_A and P_B were constructed by freely joining 50 beads *via* the spring bond force $\mathbf{F}_{ij}^{S}$, and the radius of gyration, R_g, of the P_A/P_B chains is $\sim 2.46r_c$ (corresponding to 8.0 nm). The **C** core (J_C) of the JPs was constructed by uniformly packing 26 **C** beads on the surface of a sphere of radius $R = 1.55r_c$ (corresponding to 5.0 nm). The J_C beads were restricted to move as an intact rigid body and were so closely packed that the penetration of the homopolymer beads into the cores was prevented. The **A** and **B** grafting chains (J_A and J_B) are composed of $N_{graft} = 5$ beads connected *via* the spring force $\mathbf{F}_{ij}^{S}$. (We found that the value of N_{graft} has an influence on the phase separation dynamics of the JP-compatibilized blends; see Fig. S11 of the ESI†). Note that the models of homopolymers and JPs are based on the experiment of Walther *et al.*[12] In their study, the R_g of polystyrene is $\sim$9.5 nm, and the radius of the polybutadiene core of JPs is 3–5 nm, which are comparable to the sizes of the P_A/P_B chains and J_C cores in the present study (see Section 11 of the ESI† for more discussion on the models of the JP and the P_A/P_B homopolymers).

In order to compare the behaviour of JPs with that of conventional compatibilizers, we also constructed coarse-grained models of a triblock copolymer (TCP) and two homogeneous counterparts of the JP, which are denoted by HP-I and HP-II, respectively. A model of the triblock copolymer (TCP) is shown in Fig. S2b (ESI†). Each model TCP contains an **A** end block (denoted by T_A; red), a **C** central block (denoted by T_C; purple), and a **B** block (denoted by T_B; blue). The lengths of the blocks are set to $N_{TA} = 50$, $N_{TC} = 10$ and $N_{TB} = 50$, respectively. The homogeneous particles HP-I and HP-II are both composed of a central **C** core grafted with 26 grafting chains. The grafting blocks of the HP-I particle are of component **A**, while those of the HP-II particle are of component **C** (see the insets of Fig. S2c and d, ESI†).

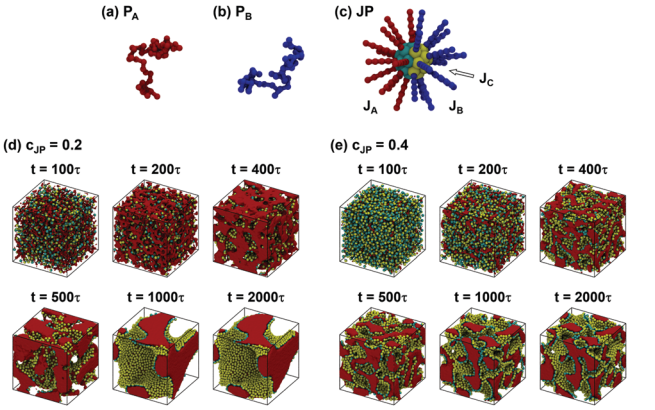

Fig. 1 (a–c) Coarse-grained models of (a) homopolymer **A** (denoted P_A), (b) homopolymer **B** (P_B) and (c) a Janus nanoparticle (JP). J_C beads connected with J_A and J_B chains are colored in cyan and yellow, respectively, to highlight the anisotropic nature of the JPs. (d and e) Morphologies of the JP-compatibilized P_A/P_B blends with (d) $c_{JP} = 0.2$ and (e) $c_{JP} = 0.4$ at various times. The JPs are sketched as small spheres with J_A (cyan) and J_B (yellow) hemispheres. Domains rich in P_A are colored in red. Domains rich in P_B are omitted for clarity.

Table 1 Interaction parameters a_{ij} (in DPD units) used in the present work

	A	B	C
A	25	75	75
B		25	75
C			25

2.3 Simulation procedure

All of our simulations were performed in cubic boxes of size $L_b = 80r_c$ with periodic boundary conditions imposed in all of the x, y, and z directions. The total number of beads was set to $3 \times L_b^3$. The following procedure was adopted. First, the homopolymers and JPs were randomly placed in the box, and the interaction parameters between unlike components were all set to 25. A preliminary simulation was conducted for 200τ to thoroughly homogenize the system (see Fig. 3a). Then, the interaction parameters between unlike components (*i.e.*, a_{AB}, a_{BC} and a_{AC}) were turned to 75, which corresponds to a thermal quench in experiments. The quench depth was sufficiently deep to induce SD. Each simulation was conducted for at least $10^4\tau$ to guarantee that the equilibrium morphology can be obtained (see Fig. 1d and e). To demonstrate that the above method provides reasonable results, we studied the phase separation dynamics of pure P_A/P_B blends (see Fig. S7–S10, ESI†). The simulation results are in good agreement with the results of theoretical predictions and experiments,[25,33,47–49] which supports the validity of the simulation method.

2.4 Structure factor

The phase separation dynamics of homopolymer blends were followed in terms of the structure factor $S(q)$, where q is the so-called scattering vector. Here, the structure factor can be obtained *via* the Fourier transform of the local composition $\varphi(\mathbf{r})$, as indicated by the following equation:

$$S(\mathbf{q}) = \left\langle \left[\sum_{\mathbf{r}} \exp(i\mathbf{q}\cdot\mathbf{r})(\varphi(\mathbf{r}) - \langle\varphi(\mathbf{r})\rangle) \right]^2 \right\rangle \Big/ L^3 \qquad (1)$$

where L is the box size; i is the symbol of imaginary number; $\langle\cdots\rangle$ denotes ensemble average; $q = 2\pi\mathbf{n}/L$, with $\mathbf{n} = (n_x, n_y, n_z)$ (n_x, n_y, n_z = 1, 2, 3...); and $\varphi(\mathbf{r})$ is defined as

$$\varphi(\mathbf{r}) = \frac{n_A(\mathbf{r}) - n_B(\mathbf{r})}{n_A(\mathbf{r}) + n_B(\mathbf{r})} \qquad (2)$$

where $n_A(\mathbf{r})$ and $n_B(\mathbf{r})$ are the number densities of the **A** and **B** beads, respectively, at position $\mathbf{r}$.[50] The $S(\mathbf{q})$ is further spherically averaged to improve the statistics in the $\mathbf{q}$ space:

$$S(q) = \sum_{q-\Delta q \le q \le q+\Delta q} S(\mathbf{q})/m(q, \Delta q) \qquad (3)$$

where $m(q, \Delta q)$ is the number of $\mathbf{q}$ vectors whose terminates are located within the spherical shell of radius q and thickness Δq. For a mixture with underlying spinodal decomposition (SD), the formation of a dominant composition fluctuation leads to the development of a peak in the $S(q)$ profile at a certain position q^*, where $1/q^*$ and $S(q^*)$ are proportional to the wavelength and amplitude, respectively, of the dominant SD wave. During the late stage, $S(q)$ can be rescaled by the characteristic length scale $1/q_1$ (proportional to the average domain size) as follows:

$$S(q) \sim (1/q_1)^3 G(q/q_1) \qquad (4)$$

where $q_1 = \sum_q qS(q) \Big/ \sum_q S(q)$ and $G(x)$ is a scaling function. This means that only one length scale ($1/q_1$) exists in the system, and the morphological evolution involves only an increase in the average domain size, while the thickness of the interfaces remains constant (self-similarity mechanism). Moreover, the growth of the average domain size during the late stage can be characterized in terms of the following exponential law:

$$q_1(t) \sim t^{-n} \qquad (5)$$

where n is a growth exponent that depends on the mechanism governing phase separation; that is, $n = 1$ when SD occurs, and $n = 1/3$ if phase separation proceeds *via* the nuclear growth (NG) or droplet SD mechanism.[33] For JP-compatibilized blends, the value of n can be obtained from the slope of the log–log profile of $q_1(t)$. A larger growth exponent indicates a steeper $q_1(t)$ curve and hence faster domain growth.

3. Results and discussion

3.1 Phase separation dynamics of JP-compatibilized blends

We first studied the phase separation dynamics of JP-compatibilized blends with various amounts of particles incorporated (see Fig. 1d and e). P_A and P_B gradually segregate into bi-continuous networks, and the Janus particles exclusively distribute at the interfaces between the P_A and P_B domains, with the J_A and J_B hemispheres in contact with the P_A and P_B phases, respectively. As a result, the growth rate of the P_A/P_B domains during the late stage was remarkably lowered (see Section 2 of the ESI†). These observations are in good agreement with those of existing studies,[12,13,23] which supports the validity of the simulation method. For example, it has been demonstrated in experiments that the increase in the c_{JP} can lead to a marked drop in the average size of the polymer domains.[12,13] Such a dependence can also be observed from Fig. 1d and e. Moreover, Huang *et al.* conducted DPD simulations to study the phase separation dynamics of homopolymer blends compatibilized by Janus spheres. They found that the Janus spheres can exclusively localize at interfaces even at the very late stage of phase separation.[23] As shown in Fig. 1d and e, the JPs are all distributed at the P_A/P_B interfaces at late times, which is consistent with the findings of Huang *et al.*

The phase separation dynamics of the JP-compatibilized blends were further characterized in terms of the structure factor $S(q)$, as shown in Fig. 2a and b. At late times, the blends with a higher particle loading ($c_{JP} = 0.4$) exhibit $S(q)$ peaks with lower intensities, which suggests that the Janus particles effectively impede the phase segregation of P_A and P_B during the late stage. However, we found that the early-time $S(q)$ peaks are more intense for the blends with $c_{JP} = 0.4$ than for those with $c_{JP} = 0.2$ (denoted by red dashed circles), which implies that the development of the dominant SD wave during the early stage is promoted by the Janus particles. Such opposite effects can be clearly viewed in Fig. 2c, which shows the peak intensity, $S(q^*)$, for blends with various particle loadings, where q^* is the position of the $S(q)$ peak. One can identify a critical time t_c before and after which $S(q^*)$ increases and

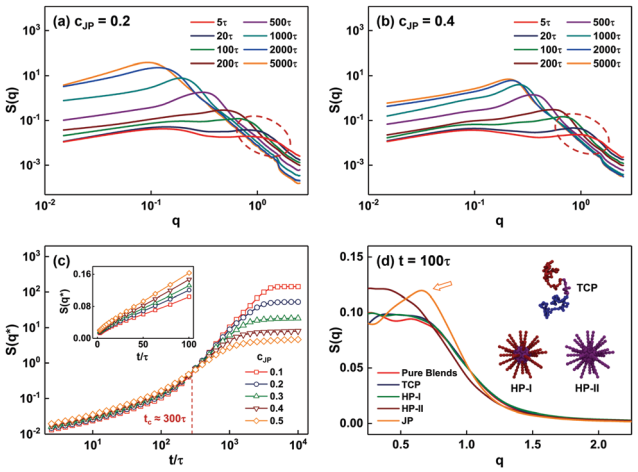

Fig. 2 Characterization of phase separation in terms of the structure factor, $S(q)$. (a and b) $S(q)$ at various times for blends with (a) c_{JP} = 0.2 and (b) c_{JP} = 0.4. Red dashed circles represent the $S(q)$ peaks at early times. (c) Peak intensity $S(q^*)$ for various particle loadings. The inset shows the $S(q^*)$ at very early times ($t \leq 100\tau$). (d) $S(q)$ profiles at $t = 100\tau$ for pure blends and blends with various additives incorporated. The insets show the coarse-grained models of the triblock copolymer (TCP), the HP-I particle, and the HP-II particle. The volume fractions of additives were all set to 0.2.

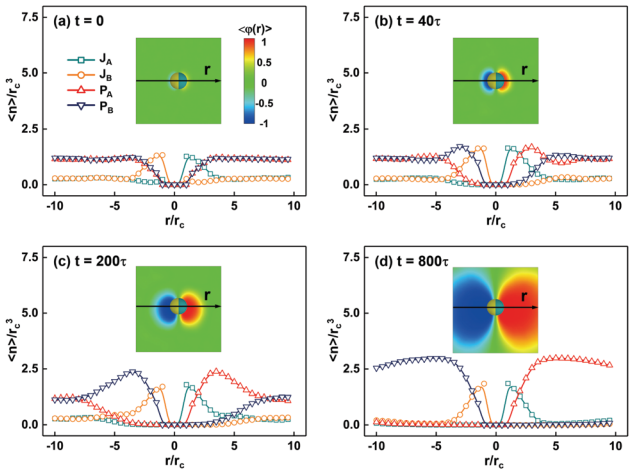

Fig. 3 Ensemble-averaged number density n of each component along the r arrows for JP-compatibilized blends with c_{JP} = 0.2 at (a) t = 0, (b) $t = 40\tau$, (c) $t = 200\tau$, and (d) $t = 800\tau$. The inset in each panel shows the ensemble-averaged composition $\varphi(\mathbf{r})$ around the Janus particles.

decreases, respectively, with increasing c_{JP}. Moreover, as shown in the inset of Fig. 2c, the growth rate of $S(q^*)$ at early times also rises with increasing c_{JP}, which confirms the promoting effect of JPs in this stage.

Interestingly, we note that other compatibilizers such as triblock copolymers and homogenous particles do not exhibit such a promoting effect at early times (see Fig. 2d). Here, we considered a triblock copolymer (TCP) with an **A** end block (colored red), a **B** end block (blue) and a **C** central block (purple) as well as two homogeneous counterparts of Janus particle: one with only **A** grafting blocks (HP-I) and the other with only **C** grafting blocks (HP-II). (Diblock copolymers are omitted because their behaviour is similar to that of the TCPs.) As shown in Fig. 2d, only the blend compatibilized by Janus particles shows a remarkable $S(q)$ peak (indicated by a red arrow) at an early time of $t = 100\tau$, and this peak is absent for systems with other additives incorporated (see Fig. S2 (ESI†) for more information).

3.2 Local microphase separation in the vicinity of Janus particles

In this subsection, the mechanism behind the unique promoting effect of Janus particles is elaborated. Since $S(q^*)$ is proportional to the amplitude of the dominant composition fluctuation, it is reasonable to expect that the Janus particles could significantly influence the spatial distributions of the **A**/**B** components in the system. Therefore, we calculated the ensemble-averaged number densities n of the P_A, P_B, J_A, and J_B components along the major axis of the Janus particles (the straight line passing through the mass centers of the J_A and J_B parts). As shown in Fig. 3a, P_A and P_B are initially uniformly mixed at every position except the interior of the J_C cores, while J_A and J_B are microphase segregated into two equally sized surface sections. After the start of phase separation, we observe the development of two **A**/**B**-rich (enrichment) regions near the J_A and J_B hemispheres, which have positive and negative compositions, respectively (Fig. 3b–d). The size $L(t)$ of the enrichment regions at various times t is obtained by evaluating the r position where the composition $\varphi(r)$ is equal to 0.9 (Fig. S3, ESI†). The influence of the particle loading (c_{JP}) on the growth rate of $L(t)$ is not remarkable at early times (Fig. S4, ESI†). At late times (Fig. 3d), all of the Janus particles are located at the interfaces, and the number densities of P_A and P_B in the enrichment regions reach the equilibrium values ($\approx 3r_c^{-3}$).

Note that the development of enrichment regions around particle surfaces can also be observed for the P_A/P_B blends with HP-I particles incorporated (Fig. S5, ESI†). However, the enrichment regions near the HP-I particles consist of only one component, whereas the enrichment regions near the J_A and J_B hemispheres of the JPs are rich in P_A and P_B, respectively. We propose that such a JP-induced local microphase separation is responsible for promoting the $S(q)$ peaks at early times for blends with higher particle loadings because the coexistence of the **A**/**B**-rich regions around the Janus particles leads to larger composition gradients at nearby positions in comparison to those in the bulk. (Note that the magnitude of $S(q^*)$ can be related to the local concentration gradient.) In contrast, the homogenous counterparts of the Janus particles cannot induce such a local microphase separation.

3.3 Development of homopolymer-rich regions

To gain clear insight into the development of **A**/**B**-rich regions, we monitored the movement of P_A/P_B and the JPs during phase separation in terms of the mean-square displacement (MSD) of the mass centers of the homopolymers and nanoparticles, which is given by

$$\mathrm{MSD} = \frac{1}{N}\sum_i [\mathbf{r}_i(t) - \mathbf{r}_i(0)]^2 \qquad (6)$$

where N is the number of homopolymers (or nanoparticles) and $\mathbf{r}_i(t)$ is the position of the mass center of the ith homopolymer

(or nanoparticle) at time t. The value of MSD is proportional to time t (*i.e.*, MSD $\sim Dt$, where D is the diffusion coefficient) if the homopolymers (or particles) are undergoing self-diffusion. As shown in Fig. S6 (ESI†), at early times ($t < t_c$), the MSD values of the JP mass centers are two to three orders of magnitude smaller than those of P_A/P_B, which suggests that early-stage movement of the Janus particles can be neglected.

Fig. 4a shows the ensemble-averaged MSD values of the homopolymer mass centers at early times for blends with various particle loadings. An increase in c_{JP} leads to an increase in the growth rate of $\langle$MSD$\rangle$, which indicates that the movement of homopolymers is promoted by the presence of Janus particles. We note that $\langle$MSD$\rangle$ is not linearly proportional to the time t during the initial stage. This result can be explained by the convective movement of the P_A/P_B beads toward their preferred JP surface regions, which can be characterized in terms of the angle θ between the velocity of a bead and the vector pointing from its position to the mass center of the nearest Janus particle (see Fig. 4b): $\cos(\theta) > 0$ suggests that the bead tends to move toward the particle, while $\cos(\theta) < 0$ indicates the opposite behavior. Fig. 4c and d shows the distributions of $\langle\cos(\theta)\rangle$ for the P_A beads in the vicinity of Janus particles at very early times. (The results for the P_B beads are omitted for conciseness). The P_A beads tend to move toward the J_A hemisphere and away from the J_B hemisphere, which leads to the formation of microphase-separated **A**/**B**-rich regions (see Fig. 4f and g) and the nonlinear growth of the $\langle$MSD$\rangle$ values at very early times.

At late times (*e.g.*, $t \geq 50\tau$), the $\langle$MSD$\rangle$ values of the homopolymer mass centers become linearly dependent on the time t because the J_A and J_B hemispheres are completely surrounded by the enrichment regions (see Fig. 4h), and the convective movement of the homopolymer beads is hence very weak (Fig. 4e). In this case, the P_A beads in the **A**-rich region show a weak tendency to move outwards due to the screening effect of the **A** beads that are already distributed in the enrichment region. Meanwhile, the P_A beads in the bulk still tend to diffuse toward the **A**-rich region, which results in the propagation of the enrichment regions from the particle surface into the bulk. We obtained the diffusion coefficient D for various particle loadings from the slope of the MSD profiles (denoted in Fig. 4a) and found that the value of D increases with increasing particle loading. This result is consistent with the putative propagation mechanism stated above.

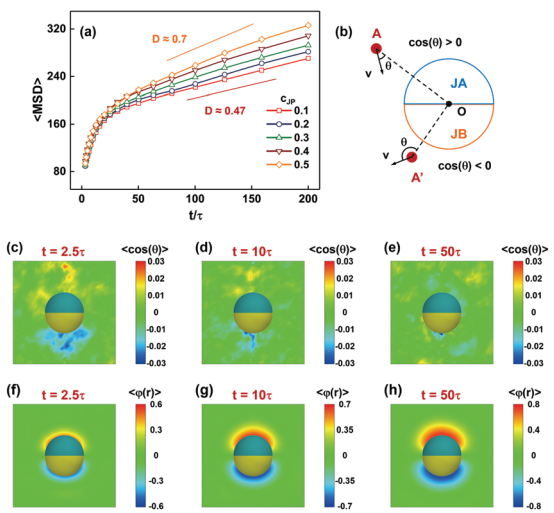

Fig. 4 (a) Ensemble-averaged MSD of the homopolymer mass centers at various times. The diffusion coefficient, D, is provided for c_{JP} = 0.1 and c_{JP} = 0.5. (b) Schematic illustration of the movement of two P_A beads (A and A′) in the vicinity of a Janus particle. (c–e) Distributions of the ensemble-averaged $\cos(\theta)$ values (defined in panel b) at (c) $t = 2.5\tau$, (d) $t = 10\tau$, and (e) $t = 50\tau$. (f–h) Ensemble-averaged composition $\varphi(\mathbf{r})$ around the Janus particles at (f) $t = 2.5\tau$, (g) $t = 10\tau$, and (h) $t = 50\tau$.

Note that the phenomenon presented in Fig. 3 and 4 can be utilized to elaborate the mechanism governing the orientation of JPs in a blending system. At the very early stage of phase separation when the two homopolymers start to segregate near the J_A and J_B hemispheres (Fig. 3a and b), the JPs are randomly oriented in the blend because the interfaces separating immiscible polymers are not yet formed. However, as the phase separation proceeds, the JPs can act as seeds to facilitate the formation of phase boundaries (Fig. 3c and d), and they tend to form orderly-oriented structures to fully cover the P_A/P_B interfaces. Consequently, a "face-ordering" transition of the JPs from random orientation at early times to parallel orientation at late times can be observed. (See Fig. S12 and S13 of the ESI† for a more detailed description.)

3.4 Mechanism behind the opposite effects of JPs

One may question why the Janus particles have opposite influences on phase separation during the early and late stages. Here, we argue that the change in the effects of the Janus particles is closely related to the conversion of the dominant transport processes of phase separation, as is schematically illustrated in Fig. 5a. As shown in the left panel of Fig. 5a, the diffusion of the homopolymers is the dominant transport process at early times except during the initial stage during which the interaction between the J_A/J_B blocks and homopolymers results in convective fluxes (see Fig. 4). In this case, the Janus particles act as promoters of phase separation, as their anisotropic structure enhances the movement of the nearby homopolymers. As phase separation enters the late stage, P_A and P_B segregate into well-defined domains (see the middle and right panels of Fig. 5a), and the phase separation is dominated by interfacial tension-driven domain coarsening, which proceeds *via* the self-similarity mechanism (see eqn (4)). During this stage, the Janus particles act as compatibilizers, as they adsorb onto the interfaces and reduce the interfacial tension.

To identify the time at which convectional domain coarsening becomes the dominant transport process, we examined the time at which phase separation starts to proceed *via* the self-similarity mechanism, which means that the morphological evolution involves only convective domain growth, whereas the interfacial thickness remains constant. As noted in eqn (4), the structure factor $S(q)$ obeys the scaling law if the blend morphology exhibits self-similarity. Therefore, we can evaluate the starting time t_s of the late stage by examining the time at which the scaling law of $S(q)$ is satisfactory since both the scaling law of $S(q)$ and

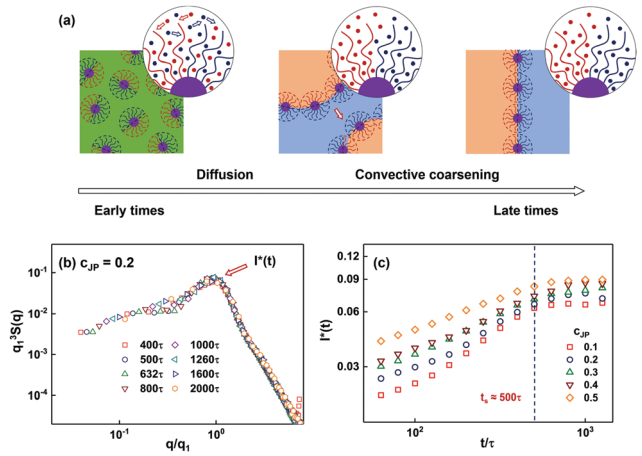

Fig. 5 Mechanism behind the opposite effects of JPs during the early and late stages. (a) Schematic illustration of the main transport processes during phase separation. The inset in the upper right corner of each panel schematically shows the spatial distributions of the P_A (red) and P_B (blue) beads around the Janus particles. The arrows in the inset of the left panel indicate the movement of the P_A and P_B beads. The red arrow in the middle panel indicates the coalescence of two P_A domains. (b) Scaled structure factor $q_1^3S(q)$ at various times for blends with a moderate particle loading of c_{JP} = 0.2 at late times. (c) Peak intensity $I^*(t)$ (see panel b) of $q_1^3S(q)$ at various c_{JP} values. The dashed line denotes the time t_s at which $I^*(t)$ reaches the equilibrium value.

convective domain growth are features of the late stage of SD.[51] As shown in Fig. 5b, the profiles of the scaled structure factor $q_1^3S(q)$ collapse onto a master curve at late times, which implies that t_s can be obtained by finding the time at which the peak intensity $I^*(t)$ becomes time invariant (see Fig. 5c). Interestingly, the value of t_s ($\approx 500\tau$) is actually comparable to the critical time t_c ($\approx 300\tau$; see Fig. 2), which effectively supports our argument that the change in the role of the Janus particles is essentially related to the switch in the dominant transport process of phase separation.

Lastly, the reason why block copolymers and homogenous particles do not show such opposite effects has been elaborated. Above, the formation of microphase-separated enrichment regions near the JPs was argued to be induced by the two opposite surface sections on the JPs. In contrast, other compatibilizers lack such inherently anisotropic structures. Note that analogous to J_A and J_B, the two end chains of the block copolymers also have different components. However, the blocks of the copolymers are uniformly mixed at the very beginning of the simulation due to the homogenizing process, and more time is required for the block copolymers to phase separate than for the polymer blends. As a result, the block copolymers cannot promote the development of a dominant SD wave in the early stage (see Fig. S2b, ESI†).

One may anticipate that the block copolymers can have faster segregation into a nucleus in a polymer melt, and then, when the temperature is decreased, behave like the JPs. However, it is well known that the segregation rate of polymers is determined by the product of the chain length N and the Flory–Huggins parameter χ.[52,53] A larger χN leads to a faster segregation of polymers. Based on such a consideration, the TCPs can segregate faster into a nucleus in a polymer melt as either (1) the Flory–Huggins parameter χ between T_A and T_B is much larger than that between P_A and P_B or (2) the chains of TCPs are extremely longer than the homopolymer chains. Note that in the present work, the T_A (T_B) blocks and the P_A (P_B) polymers are composed of the identical components, which means that the χ between the T_A and T_B blocks is the same as that between P_A and P_B. On the other hand, the molecular weight of the triblock copolymers used for improving the miscibility is usually smaller than that of the homopolymers.[54,55] Therefore, the microphase separation of the triblock copolymers should be slower than the macrophase separation of the homopolymer blends. It is hence expected that the early-stage enhancement of polymer blend segregation can hardly be observed when the block copolymers are incorporated.

Note that as shown in Fig. 2d, the blend with HP-II particles incorporated also shows high $S(q)$ values in the small q region during the early stage in comparison to those of pure blends or blends with TCPs and HP-I particles incorporated. This difference is due to the improved movement of the homopolymers, which tend to move away from the HP-II particles, whose grafting blocks are immiscible with both P_A and P_B. Nevertheless, the HP-II particles lack an anisotropic structure and hence cannot induce local microphase separation during the early stage like the Janus particles do. We also note that the mechanisms exploited in this work are not limited to the so-called "SBM" JPs, which consists of a cross-linked spherical core with two types of polymeric chains emanating from it, but also apply to JPs with various structures such as Janus rods and Janus disks.[1] This is because the unique behavior of JPs at the early stage of SD is essentially related to the inherently anisotropic nature of JPs, and the specific structure of JPs does not remarkably influence the underlying mechanisms in general.

3.5 Discussion

Over the past few decades, the influences of compatibilizers on the phase separation dynamics of polymer blends have been intensively investigated, and most of the prior works focused on the retarding effect of compatibilizers on phase separation. For example, Jo *et al.* performed Monte Carlo simulations to investigate the influence of block copolymers on the phase separation dynamics of homopolymer blends.[54,56,57] Their works suggested that the segregation of the block copolymers at interfaces can minimize the number of unfavourable interactions and reduce the interfacial tension, thereby lowering the growth rate of polymer domains at the late stage of phase separation. For homogeneous particles preferred by one of the unlike homopolymers, Laradji *et al.* demonstrated that the pinning effect of filler particles leads to a decrease in the domain growth rate when the nanoparticles are annealed and are mobile.[58] Lastly, for nanoparticles expelled by both polymers, the particles can act as a particulate surfactant and play a similar role to block copolymers.[59] Although the retarding effects of block copolymers and nanoparticles are weaker at early times due to the larger proportion of interfaces than polymer domains, the block copolymers and nanoparticles can still impede phase separation during the early stage. This fact is the basis of the long-standing

belief that compatibilizers can impede the phase separation dynamics during the full course of SD.

However, in the present work, we discovered that such a physical phenomenon does not apply to JPs, as they can promote phase separation during the early stage, as indicated by the remarkable peaks in the structure factor $S(q)$ at early times. The key is that the anisotropic structure of the Janus particles leads to the movement of the homopolymers toward their preferred JP surface regions, which further results in the formation of microphase-separated homopolymer-rich regions and hence a larger concentration gradient in the vicinity of the Janus particles. This JP-induced local microphase separation is responsible for the promotion of phase separation during the early stage. Such an inherent anisotropy is apparently absent in traditional compatibilizers. Considering the behavior of other compatibilizers such as block copolymers and homogeneous counterparts of JPs which impede phase separation during the full course of SD (as demonstrated in this work), the opposite effects of JPs at the early and late stages of SD not only offer a novel insight into the roles of compatibilizers, but also indicate a particular and important feature of JPs which has not been exploited before. Therefore, it is expected that the present study could offer novel results which help to deepen our understanding on the roles of compatibilizers. (For more discussion on the mechanism behind JP-induced local microphase separation, see Section 8 of the ESI†).

Finally, we wish to emphasize that the novel mechanism exploited here may have important implications for the phase separation of polymer blends of technological relevance, such as polymer alloys with enhanced mechanical properties,[13,60] as well as of the mixtures of donor and acceptor polymers that are promising components in organic solar cells.[61–63] For example, studying the influence of compatibilizers on the growth rate of phase-separated structures is of critical value because one may intentionally terminate the SD process at a certain time in order to obtain materials with desired structures and properties. In this work, we found that the favourable interactions between homopolymers and their preferred JP surface regions could facilitate the directed movement of the homopolymers toward the surface regions of JPs, which suggests that the growth rate of structures can be controlled by introducing specific interactions such as electrostatic forces and hydrogen bonding into a system in order to tune the strength of diffusional fluxes. (Note that the diffusional flux is the dominant transport process at the early stage of SD). Considering the growing number of studies that utilize JPs as compatibilizers for high-performance polymer alloys, our findings can be useful for researchers working on the preparation of polymer alloys with tunable structures. In addition, we believe that this work also has implications for the design of functional materials based on polymer blends. For instance, the mixtures of donor and acceptor polymers are important components in all-polymer solar cells, and their photovoltaic properties (*e.g.*, short-circuit current densities) can be optimized by decreasing the average size of polymer domains as well as increasing the area of interfaces between donor and acceptor polymer phases.[62] Since the presence of JPs leads to decreased average domain size (Fig. 1) and increased interfacial area (note that JPs are exclusively located at the interfaces), it is reasonable to expect that the performance of photovoltaic materials based on donor/acceptor polymer blends can be optimized by introducing JPs into a blending system and changing the interactions between the JP surfaces and homopolymers.

4. Conclusions

The phase separation dynamics of homopolymer blends compatibilized by Janus nanoparticles (JPs) were studied *via* dissipative particle dynamics simulations. In contrast to other compatibilizers such as triblock copolymers and homogenous nanoparticles, the JPs uniquely exhibit opposite effects on the phase separation dynamics during the early and late stages of spinodal decomposition, *i.e.*, they promote phase separation at early times but impede it at late times. During the early stage, the preferred movement of the homopolymers toward the opposite JP surface regions leads to the formation of microphase-separated enrichment regions, which further results in enhanced structure factor peaks at early times. During the late stage, the Janus particles are located at the interfaces between the homopolymer domains, which reduce the interfacial tension and impede the growth of domains. The present work sheds light on the behavior of Janus nanoparticles during the phase separation of polymer blends and offers useful insights for the design and preparation of novel materials.

Conflicts of interest

There are no conflicts of interest to declare.

Acknowledgements

This work was supported by the National Natural Science Foundation of China (No. 51621002, 21474029, and 21774032). Support from Projects of Shanghai municipality (No. 16520721900) and the Fundamental Research Funds for the Central Universities (222201714042) is also appreciated.

References

1 A. Walther and A. H. E. Müller, *Chem. Rev.*, 2013, **113**, 5194–5261.
2 P. Cai, Y. Hong, S. Ci and Z. Wen, *Nanoscale*, 2016, **8**, 20048–20055.
3 S. Yan, H. Zou, S. Chen, N. Xue and H. Yang, *Chem. Commun.*, 2018, **54**, 10455–10458.
4 J. Liu, H.-L. Guo and Z.-Y. Li, *Nanoscale*, 2016, **8**, 19894–19900.
5 M. N. Popescu, W. E. Uspal, C. Bechinger and P. Fischer, *Nano Lett.*, 2018, **18**, 5345–5349.
6 L. Wang, M. N. Popescu, F. Stavale, A. Ali, T. Gemming and J. Simmchen, *Soft Matter*, 2018, **14**, 6969–6973.
7 Y. Ju, H. Zhang, J. Yu, S. Tong, N. Tian, Z. Wang, X. Wang, X. Su, X. Chu, J. Lin, Y. Ding, G. Li, F. Sheng and Y. Hou, *ACS Nano*, 2017, **11**, 9239–9248.

8 T. Truong-Cong, E. Millart, L. T. C. Tran, H. Amenitsch, G. Frebourg, S. Lesieur and V. Faivre, *Nanoscale*, 2018, **10**, 3654–3662.
9 Z. Wang, D. Shao, Z. Chang, M. Lu, Y. Wang, J. Yue, D. Yang, M. Li, Q. Xu and W.-F. Dong, *ACS Nano*, 2017, **11**, 12732–12741.
10 Y. Xiong, M. Li, H. Liu, Z. Xuan, J. Yang and D. Liu, *Nanoscale*, 2017, **9**, 1811–1815.
11 H. Wang, S. Li, L. Zhang, X. Chen, T. Wang, M. Zhang, L. Li and C. Wang, *Nanoscale*, 2017, **9**, 14322–14326.
12 A. Walther, K. Matussek and A. H. E. Müller, *ACS Nano*, 2008, **2**, 1167–1178.
13 R. Bahrami, T. I. Löbling, A. H. Gröschel, H. Schmalz, A. H. E. Müller and V. Altstädt, *ACS Nano*, 2014, **8**, 10048–10056.
14 H. Wang, W. Dong and Y. Li, *ACS Macro Lett.*, 2015, **4**, 1398–1403.
15 K. C. Bryson, T. I. Löbling, A. H. E. Müller, T. P. Russell and R. C. Hayward, *Macromolecules*, 2015, **48**, 4220–4227.
16 T. Parpaite, B. Otazaghine, A. S. Caro, A. Taguet, R. Sonnier and J. M. Lopez-Cuesta, *Polymer*, 2016, **90**, 34–44.
17 H. Wang, Z. Fu, X. Zhao, Y. Li and J. Li, *ACS Appl. Mater. Interfaces*, 2017, **9**, 14358–14370.
18 R. Bahrami, T. I. Löbling, H. Schmalz, A. H. E. Müller and V. Altstädt, *Polymer*, 2017, **109**, 229–237.
19 W. Xu, J. Chen, S. Chen, Q. Chen, J. Lin and H. Liu, *Ind. Eng. Chem. Res.*, 2017, **56**, 14060–14068.
20 Q. Yang and K. Loos, *Polym. Chem.*, 2017, **8**, 641–654.
21 H. Nie, X. Liang and A. He, *Macromolecules*, 2018, **51**, 2615–2620.
22 B. P. Binks and P. D. I. Fletcher, *Langmuir*, 2001, **17**, 4708–4710.
23 M. Huang, Z. Li and H. Guo, *Soft Matter*, 2012, **8**, 6834–6845.
24 M. Huang and H. Guo, *Soft Matter*, 2013, **9**, 7356–7368.
25 J. W. Cahn, *J. Chem. Phys.*, 1965, **42**, 93–99.
26 X. Zhang, Z. Wang and C. C. Han, *Macromolecules*, 2006, **39**, 7441–7445.
27 L.-T. Yan and X.-M. Xie, *Macromolecules*, 2006, **39**, 2388–2397.
28 Z. Chen, X. Wang, Y. Qi, S. Yang, J. A. N. T. Soares, B. A. Apgar, R. Gao, R. Xu, Y. Lee, X. Zhang, J. Yao and L. W. Martin, *ACS Nano*, 2016, **10**, 10237–10244.
29 T. Hashimoto, M. Itakura and M. Hasegawa, *J. Chem. Phys.*, 1986, **85**, 6118–6128.
30 T. Hashimoto, M. Itakura and N. Shimidzu, *J. Chem. Phys.*, 1986, **85**, 6773–6786.
31 K. Kawasaki, *Prog. Theor. Phys.*, 1977, **57**, 826–839.
32 K. Kawasaki and T. Ohta, *Prog. Theor. Phys.*, 1978, **59**, 1406.
33 R. Shimizu and H. Tanaka, *Nat. Commun.*, 2015, **6**, 7407.
34 R. D. Groot and P. B. Warren, *J. Chem. Phys.*, 1997, **107**, 4423–4435.
35 A. Alexeev, W. E. Uspal and A. C. Balazs, *ACS Nano*, 2008, **2**, 1117–1122.
36 L.-T. Yan, N. Popp, S.-K. Ghosh and A. Böker, *ACS Nano*, 2010, **4**, 913–920.
37 H.-M. Ding and Y.-Q. Ma, *Nanoscale*, 2012, **4**, 1116–1122.
38 I. Salib, X. Yong, E. J. Crabb, N. M. Moellers, G. T. McFarlin, O. Kuksenok and A. C. Balazs, *ACS Nano*, 2013, **7**, 1224–1238.
39 P. Chen, Z. Huang, J. Liang, T. Cui, X. Zhang, B. Miao and L.-T. Yan, *ACS Nano*, 2016, **10**, 11541–11547.
40 Q.-S. Xia, H.-M. Ding and Y.-Q. Ma, *Nanoscale*, 2017, **9**, 8982–8989.
41 T. Jiang, L. Wang, S. Lin, J. Lin and Y. Li, *Langmuir*, 2011, **27**, 6440–6448.
42 Z. Xu, J. Lin, Q. Zhang, L. Wang and X. Tian, *Polym. Chem.*, 2016, **7**, 3783–3811.
43 Q. Li, L. Wang and J. Lin, *Phys. Chem. Chem. Phys.*, 2017, **19**, 24135–24145.
44 Q. Zhang, J. Lin, L. Wang and Z. Xu, *Prog. Polym. Sci.*, 2017, **75**, 1–30.
45 Y. Zhou, M. Huang, T. Lu and H. Guo, *Macromolecules*, 2018, **51**, 3135–3148.
46 A. Singh, A. Chakraborti and A. Singh, *Soft Matter*, 2018, **14**, 4317–4326.
47 H. L. Snyder and P. Meakin, *J. Polym. Sci., Polym. Symp.*, 1985, **73**, 217–239.
48 E. D. Siggia, *Phys. Rev. A: At., Mol., Opt. Phys.*, 1979, **20**, 595–605.
49 T. Koga and K. Kawasaki, *Phys. Rev. A: At., Mol., Opt. Phys.*, 1991, **44**, R817–R820.
50 R. Malik, C. K. Hall and J. Genzer, *Macromolecules*, 2013, **46**, 4207–4214.
51 H. Furukawa, *Adv. Chem. Phys.*, 1985, **34**, 703–750.
52 P. J. Flory, *J. Chem. Phys.*, 1942, **10**, 51–61.
53 M. L. Huggins, *J. Chem. Phys.*, 1941, **9**, 440.
54 W. H. Jo and S. H. Kim, *Macromolecules*, 1996, **29**, 7204–7211.
55 H. Ruckdäschel, J. K. W. Sandler, V. Altstädt, C. Rettig, H. Schmalz, V. Abetz and A. H. E. Müller, *Polymer*, 2006, **47**, 2772–2790.
56 S. H. Kim, W. H. Jo and J. Kim, *Macromolecules*, 1996, **29**, 6933–6940.
57 S. H. Kim, W. H. Jo and J. Kim, *Macromolecules*, 1997, **30**, 3910–3915.
58 M. Laradji and G. MacNevin, *J. Chem. Phys.*, 2003, **119**, 2275–2283.
59 M. J. A. Hore and M. Laradji, *J. Chem. Phys.*, 2007, **126**, 244903.
60 H. Pernot, M. Baumert, F. Court and L. Leibler, *Nat. Mater.*, 2002, **1**, 54–58.
61 R. Lecover, N. Williams, N. Markovic, D. H. Reich, D. Q. Naiman and H. E. Katz, *ACS Nano*, 2012, **6**, 2865–2870.
62 N. Zhou, A. S. Dudnik, T. I. N. G. Li, E. F. Manley, T. J. Aldrich, P. Guo, H.-C. Liao, Z. Chen, L. X. Chen, R. P. H. Chang, A. Facchetti, M. Olvera de la Cruz and T. J. Marks, *J. Am. Chem. Soc.*, 2016, **138**, 1240–1251.
63 N. Balar, Y. Xiong, L. Ye, S. Li, D. Nevola, D. B. Dougherty, J. Hou, H. Ade and B. T. O'Connor, *ACS Appl. Mater. Interfaces*, 2017, **9**, 43886–43892.

